diabetes
American Diabetes Association

PRMT4 Facilitates White Adipose Tissue Browning and Thermogenesis by Methylating PPARγ

Yi Zhong, Yilong Wang, Xiaoguang Li, Haojie Qin, Shu Yan, Caijun Rao, Di Fan, Duqiu Liu, Fei Deng, Yanli Miao, Ling Yang, and Kai Huang

Diabetes 2023;72(8):1095–1111 | https://doi.org/10.2337/db22-1016

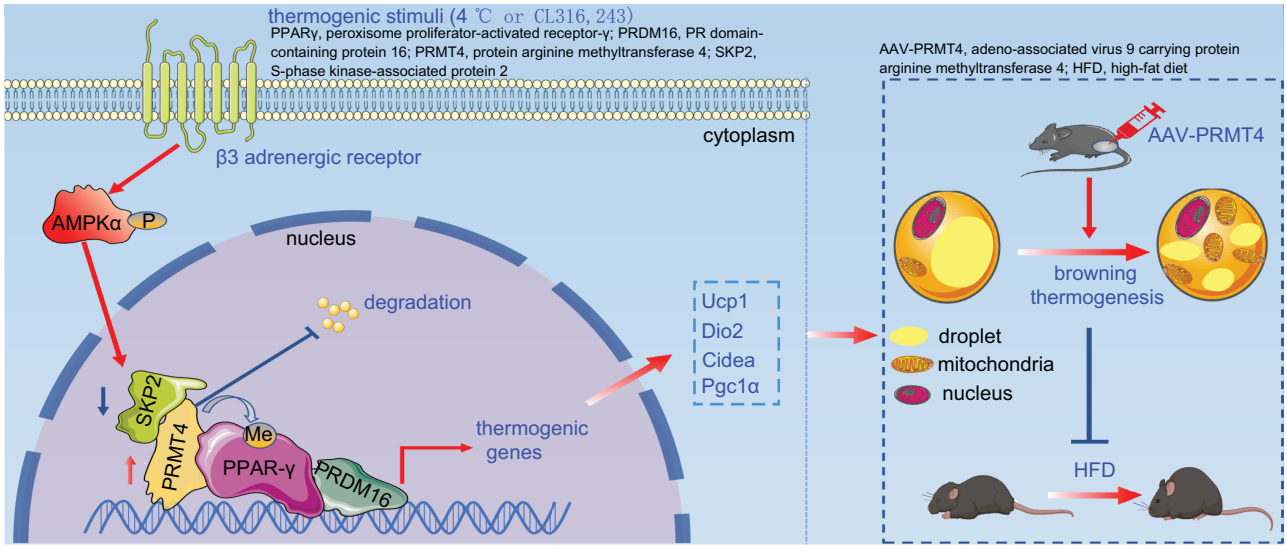

PRMT4 Facilitates White Adipose Tissue Browning and Thermogenesis by Methylating PPARγ

Yi Zhong,[1,2] Yilong Wang,[3] Xiaoguang Li,[1] Haojie Qin,[1,4] Shu Yan,[5] Caijun Rao,[6] Di Fan,[1,4] Duqiu Liu,[1,7] Fei Deng,[8] Yanli Miao,[9] Ling Yang,[1,2] and Kai Huang[1,4,10,11]

Diabetes 2023;72:1095–1111 | https://doi.org/10.2337/db22-1016

Obesity is a global health threat, and the induction of white adipose tissue (WAT) browning presents a promising therapeutic method for it. Recent publications revealed the essential role of protein arginine methyltransferase 4 (PRMT4) in lipid metabolism and adipogenesis, but its involvement in WAT browning has not been investigated. Our initial studies found that the expression of PRMT4 in adipocytes was upregulated in cold-induced WAT browning but downregulated in obesity. Besides, PRMT4 overexpression in inguinal adipose tissue accelerated WAT browning and thermogenesis to protect against high-fat diet–induced obesity and metabolic disruptions. Mechanistically, our work demonstrated that PRMT4 methylated peroxisome proliferator-activated receptor-γ (PPARγ) on Arg240 to enhance its interaction with the coactivator PR domain-containing protein 16 (PRDM16), leading to the increased expression of thermogenic genes. Taken together, our results uncover the essential role of the PRMT4/PPARγ/PRDM16 axis in the pathogenesis of WAT browning.

ARTICLE HIGHLIGHTS

- Protein arginine methyltransferase 4 (PRMT4) expression was upregulated during cold exposure and negatively correlated with body mass of mice and humans.
- PRMT4 overexpression in inguinal white adipose tissue of mice improved high-fat diet–induced obesity and associated metabolic impairment due to enhanced heat production.
- PRMT4 methylated peroxisome proliferator-activated receptor-γ on Arg240 and facilitated the binding of the coactivator PR domain-containing protein 16 to initiate adipose tissue browning and thermogenesis.
- PRMT4-dependent methylation of peroxisome proliferator-activated receptor-γ on Arg240 is important in the process of inguinal white adipose tissue browning.

Obesity is defined as a clinical syndrome with excessive adipose deposition in the subcutaneous tissue or visceral organs. It is estimated that >10% of adults are disturbed by obesity and its related metabolic disorders, thus making it a serious public health concern (1). Obesity, resulting from the imbalance between energy storage and expenditure, is intimately related to energy homeostasis in adipose tissue. Two types of

[1]Clinic Center of Human Gene Research, Union Hospital, Tongji Medical College, Huazhong University of Science and Technology, Wuhan, China
[2]Division of Gastroenterology, Union Hospital, Tongji Medical College, Huazhong University of Science and Technology, Wuhan, China
[3]Department of Cardiology, The First Affiliated Hospital of Sun Yat-sen University, Guangzhou, China
[4]Department of Cardiology, Union Hospital, Tongji Medical College, Huazhong University of Science and Technology, Wuhan, China
[5]Heart Center and Institute of Pediatrics, Guangzhou Women and Children's Medical Center, Guangzhou Medical University, Guangzhou, China
[6]Department of Geriatrics, Tongji Hospital, Tongji Medical College, Huazhong University of Science and Technology, Wuhan, China
[7]Liyuan Cardiovascular Center, Tongji Medical College, Huazhong University of Science and Technology, Wuhan, China
[8]Department of Urology, The Second Xiangya Hospital, Central South University, Hunan, China
[9]Department of Cardiology, The First Affiliated Hospital of Zhengzhou University, Zhengzhou, China
[10]Hubei Key Laboratory of Metabolic Abnormalities and Vascular Aging, Huazhong University of Science and Technology, Wuhan, China
[11]Hubei Clinical Research Center of Metabolic and Cardiovascular Disease, Huazhong University of Science and Technology,Wuhan, China

Corresponding authors: Yanli Miao, miaounion2020@163.com, Ling Yang, hepayang@163.com, or Kai Huang, unionhuangkai@163.com

Received 12 December 2022 and accepted 10 May 2023

This article contains supplementary material online at https://doi.org/10.2337/figshare.22929269.

Y.Z., Y.W., and X.L. contributed equally to this work.

adipose tissue have been identified in humans, including white adipose tissue (WAT) and brown adipose tissue (BAT) (2). WAT conserves triglycerides for energy storage, while BAT, with abundant mitochondria and specifically expressed uncoupling protein-1 (UCP1) (3), participates in the thermogenic process to ensure energy expenditure. Two kinds of thermogenic adipocytes have been uncovered, including classical brown and beige adipocytes. Beige adipocytes can be developed within WAT depots in cold-exposed or β-adrenergic–stimulated scenarios, an integral process termed "WAT browning" (2,4). Decreased BAT content or disrupted BAT function was constantly observed in obesity, and the acceleration of WAT browning may present a promising therapeutic strategy for obesity (5).

The molecular machinery of WAT browning has been intensively investigated for decades (2,3), and recent publications revealed that various transcription factors were involved. Peroxisome proliferator-activated receptor-γ (PPARγ) is one of the most investigated transcription factors in white adipocytes and beige/brown adipocytes differentiation (6–10). Previous studies indicated that the role of PPARγ in adipocytes was largely decided by the recruited coregulators (7). It has been validated that PPARγ interacted with early B-cell factor-2 (EBF2), PR domain-containing protein 16 (PRDM16), or PPARγ coactivator 1α (PGC1α) to facilitate WAT browning (11). Interestingly, the exact cofactors recruited by PPARγ were intimately regulated by their posttranslational events. Data from the previous publications revealed that various types of posttranslational modifications, including deacetylation, phosphorylation, sumoylation, and ubiquitination (12), participated in the modulation of PPARγ activity. However, the methylation in PPARγ, a unique type of posttranslational modification, has not been investigated (12).

Protein arginine methyltransferase 4 (PRMT4), a member of the protein arginine methyltransferases (PRMT) family, also termed as coactivator-associated arginine methyltransferase 1 (CARM1), plays a pivotal role in transcriptional regulation (13). Previous data showed that PRMT4 catalyzes the methylation of arginine residues in its substrates to modulate the activity of various transcription regulators (13,14). It has been validated that the enzymatic activity of PRMT4 was involved in multiple bioprocesses, including skeletal muscle differentiation, cell fate determination, and myeloid differentiation (14–16). The role of PRMT4 in lipid metabolism and adipogenesis was recently recognized (17–20), but its involvement in WAT browning has not been investigated. In this study, we identified PPARγ as a new methylation substrate of PRMT4, and further investigations demonstrated that PRMT4-mediated methylation of PPARγ was critical for the recruitment of PRDM16 to accelerate WAT browning and thermogenesis.

RESEARCH DESIGN AND METHODS

Human Participants

The subcutaneous adipose samples used in this study were obtained from patients at the Union Hospital, Tongji Medical College, Huazhong University of Science and Technology. All patients provided informed consent. This study was approved by the Institutional Ethics Board of Tongji Medical College, Huazhong University of Science and Technology (2020-S092), and complied with the ethical norms of the 1975 Declaration of Helsinki.

Animals

All animal procedures were approved by the Tongji Medical College of Huazhong University of Science and Technology Institutional Animal Care and Use Committee (S2932) and conformed to the *Guide for the Care and Use of Laboratory Animals* published by the U.S. National Institutes of Health. Animals were purchased from Weitonglihua Co., Ltd. (Beijing, China) and housed in an animal facility on a 12-h light/12-h dark cycle at a room temperature of 22–23°C and humidity of 40–60%, with free access to food and water. For inguinal WAT (iWAT)-specific PRMT4 overexpression and knockdown in vivo, adeno-associated virus 9 (AAV9) carrying PRMT4 (AAV-PRMT4) or shRNA against PRMT4 (AAV-shPRMT4) was administered via bilateral subcutaneous injections at six points on each side of the inguinal area. AAV9-carrying negative control (AAV-NC) and scramble shRNA (AAV-shNC) were used as controls. For the high-fat diet (HFD) model (60%; Research Diet, D12492), mice were injected with AAV-NC or AAV-PRMT4 at 6 weeks of age. At 2 weeks after the AAV injection, when ectopic PRMT4 expression was considered stable, mice were fed the HFD for 8 weeks. Food intake and body weight were measured weekly. Glucose tolerance test (GTT) and insulin tolerance test (ITT) were performed after 6 and 7 weeks of continuous HFD feeding, respectively. Metabolism-related parameters were measured 1 week later using a comprehensive laboratory animal monitoring system (CLAMS, Columbus Instruments). After 8 weeks, the mice were sacrificed under anesthesia, and serum and tissues were collected for further analysis. For cold exposure, 2 weeks after the AAV9 injection, the mice were subjected to a cold challenge (4°C) for 24 h. For the reverse experiment, T0070907 (a specific inhibitor of PPARγ, 2 mg/kg; Selleck, S2871) was intraperitoneally injected 1 day before cold exposure. The sequence of mouse shPRMT4 is as follows: *m*-shPRMT4, 5′-TCAGGGACATGTCTGCTTATT-3′.

Isolation of Primary Stromal Vascular Fraction Cells From iWAT and In Vitro Differentiation

Stromal vascular fraction (SVF) cells were isolated from the inguinal adipose pad of male 6-week-old mice, as described previously (21). For differentiation, insulin (10 μg/mL; Sigma-Aldrich, 1342106), 3-isobutyl-1-methylxanthine (0.5 mmol/L; Sigma-Aldrich, I5879), dexamethasone (2 μmol/L; Sigma-Aldrich, D1756), and rosiglitazone (2.5 μmol/L; Sigma-Aldrich, R2408) were added to the culture medium after reaching confluence for 2 days (day 0). After 2 days, 10 μg/mL insulin and 2.5 μmol/L rosiglitazone continued to be incubated with SVF cells. On day 6, when primary adipocytes

matured, cells were infected with adenovirus for 48 h and then treated with or without CL316,243 (2 μmol/L; Sigma-Aldrich, C5976) for 4 h. All cells were maintained at 37°C in a humidified atmosphere of 5% CO_2.

Virus Preparation

Adenovirus was used to infect SVF cells in vitro, whereas the recombinant AAV system was used to transduce iWAT in vivo. All viruses were provided by OBiO Technology Ltd., Shanghai, China.

GTT and ITT

For the GTT, after 16–18 h of starvation in both groups, mice were injected intraperitoneally with glucose (2 g/kg body wt; Sigma-Aldrich, D9434), and blood glucose levels were measured at 0, 15, 30, 60, 90, and 120 min. One week after the GTT measurement, insulin (0.75 unit/kg body wt; Sigma-Aldrich, 1342106) was injected intraperitoneally following starvation for 4 h, and the blood glucose levels were measured at 0, 15, 30, 60, 90, and 120 min after the insulin injection.

Lipid Analyses

In accordance with the manufacturer's instructions, lipid levels in liver tissues or serum were measured using commercial assay kits for triglyceride (Wako, 290-63701) and free fatty acid (Wako, 294-63601).

Metabolic Analysis

The metabolic analysis was performed using the CLAMS for 24 h at 23°C or 4°C under a daily 12-h light/dark cycle.

Plasmid Construction

The plasmids used in this study were purchased from Addgene (Watertown, MA) or MiaolingBio (Wuhan, China). The mutated forms of PRMT4 ($PRMT4^{E266Q}$) and PPARγ ($PPAR\gamma^{R240A}$) were constructed by MiaolingBio (Wuhan, China) and validated by gene sequencing (Tsingke Biotechnology Co., Ltd., Wuhan, China).

Histological Analysis

Hematoxylin and eosin (H&E) staining, immunohistochemistry (IHC), Oil Red O staining, and immunofluorescence were performed as previously described (21). Images were acquired using NanoZoomer S360 (Hamamatsu Photonics, Fukuoka City, Japan). The antibodies used for IHC included PRMT4 (1:500; Bethyl Laboratories, A300-421A, RRID: AB_2068452) and UCP1 (1:500; Abcam, ab10983, RRID: AB_2241462). The antibodies used for immunofluorescence included CD68 (1:500; Proteintech, 28058-1-AP, RRID: AB_2881049), platelet-derived growth factor receptor-α (1:1,000; Abcam, ab203491, RRID:AB_2892065), Flag (1:100; Sigma-Aldrich, F1804, RRID:AB_262044), adiponectin (1:200; Proteintech, 21613-1-AP, RRID:AB_2878891), PRMT4 (1:400; Bethyl Laboratories, A300-421A, RRID: AB_2068452), and CD31 (1:100; Cell Signaling Technology, 3528, RRID:AB_2160882).

Western Blotting

Tissue or cell samples were lysed with radioimmunoprecipitation assay lysis buffer. After the concentration was determined, the proteins were subjected to SDS-PAGE and transferred onto a polyvinylidene fluoride membrane. The membranes were blocked 1 h at room temperature and were incubated with the following antibodies: PRMT4 (1:5,000; Bethyl Laboratories, A300-421A, RRID:AB_2068452), protein arginine methyltransferase 1 (PRMT1; 1:1,000; Proteintech, 11279-1-AP, RRID:AB_2171319), asymmetric di-methyl arginine (ADMA, 1:1,000; Cell Signaling Technology, 13522, RRID: AB_2665370), β-actin (1:5,000; Abcam, ab8226, RRID: AB_306371), GAPDH (1:1,000; Proteintech, 60004-1-Ig, RRID: AB_2107436), β-tubulin (1:5,000; Abcam, ab6046, RRID: AB_2210370), PPARγ (1:1,000; Cell Signaling Technology, 2443, RRID:AB_823598), PRDM16 (1:1,000; Abcam, ab106410, RRID:AB_10866455), H3R17Me2 (1:1,000; ABclonal, A2421, RRID:AB_2764339), UCP1 (1:1,000; Abcam, ab10983, RRID: AB_2241462), Flag (1:2,000; Sigma-Aldrich, F1804, RRID: AB_262044), His (1:5,000; Proteintech, 66005-1-Ig, RRID: AB_11232599), hemagglutinin (1:2,000; Proteintech, 51064-2-AP, RRID:AB_11042321), S-phase kinase-associated protein 2 (1:1,000; Invitrogen, 32-3300, RRID:AB_2533074), AMPKα (1:1,000; Cell Signaling Technology, 2532, RRID: AB_330331), phosphorylated (p)-AMPKα (1:1,000; Cell Signaling Technology, 2535, RRID:AB_331250), fibroblast growth factor 2 (1:1,000; Abcam, ab171941, RRID: AB_2629460), amyloid protein-binding protein (APPBP) 2 (1:1,000, Proteintech, 12409-1-AP, RRID:AB_2918029), and PGC1α (1:1,000, Abcam, ab191838, RRID:AB_2721267). Chemiluminescence signals were detected using a Clinx imaging system (Shanghai, China).

Coimmunoprecipitation Assay

Following overnight incubation at 4°C with the specified antibodies or IgG (Cell Signaling Technology, 3900 and 5415), protein A/G magnetic beads (MedChemExpress, HY-K0202) were added to the protein samples, which were then incubated for an additional 2 h on a rotator. The centrifuged immunoprecipitates were washed six times with wash buffer (150 mmol/L NaCl, 20 mmol/L Tris-HCl, pH 7.5, 5% glycerol, 1 mmol/L $MgCl_2$, and 1 mmol/L EDTA). The pellets were boiled before the immunoblotting analysis.

Recombinant Protein Expression and Purification

Plasmids encoding recombinant *PRMT4-His* were transfected into human embryonic kidney 293T (HEK293T) cells (ATCC, RRID: CVCL_1926), and the cells were lysed 48 h after transfection and purified using nickel-nitrilotriacetic acid agarose beads (Sigma-Aldrich, H0537). PPARγ-Flag (wild-type [WT]) or $PPAR\gamma^{R240A}$-Flag (mutant [mut]) proteins were affinity purified from the extracts of HEK293T cells expressing Flag-tagged PPARγ or $PPAR\gamma^{R240A}$. The PPARγ-Flag proteins were immunoprecipitated using Flag-M2

affinity gel (Sigma-Aldrich, A2220), washed six times, and the bound materials were eluted in the presence of 0.2 mg/mL Flag peptide.

Chromatin Immunoprecipitation Assay

The chromatin immunoprecipitation assay (ChIP) assay was performed using a commercially available kit (Millipore, 17-295) in accordance with the manufacturer's guidelines. Briefly, adipose tissues were subjected to cross-linking, quenching, lysis, and sonication in turn, then the lysates were centrifuged and incubated with specific antibodies for 12 h and protein A/G Sepharose (Abcam, ab193262) for extra 2 h on a rotator at 4°C. The beads were washed and eluted. The supernatant was reverse–cross-linked overnight at 65°C and then digested for another 4 h at 55°C. Quantitative PCR (qPCR) was performed after ChIP, and the input DNA was purified. The following primers were used for ChIP assays: *m*-UCP1 (ChIP), forward: 5′-CCTGGCTGTCCTAGAACT-3′; reverse: 5′-GCAGTGATGAGCAGTCAG-3′.

In Vitro Methylation Assay

An in vitro methyltransferase assay was performed using PPARγ-Flag or PPARγ^{R240A}-Flag proteins and purified recombinant PRMT4-His proteins. Briefly, 1 μg of PPARγ-Flag (PPARγ-WT) or PPARγ^{R240A}-Flag (PPARγ-mut) proteins was incubated with 1 μg of PRMT4-His and 10 μmol/L *S*-adenosyl-L-methionine (Sigma-Aldrich, A4377) in the presence or absence of TP-064 (a selective inhibitor of PRMT4, 10 μmol/L; MedChemExpress, HY-114965) in methylation buffer (25 mmol/L NaCl, 25 mmol/L Tris-HCl, pH 8.8) for 2 h at 30°C. Proteins were subjected to a coimmunoprecipitation (co-IP) assay with an anti-Flag antibody.

Mass Spectrometry Identification of PPARγ Methylation Sites

Purified methylated PPARγ proteins were separated by SDS-PAGE, stained with Coomassie blue, cut into pieces, and further destained until colorless. The samples were reduced with 10 mmol/L 1,4-dithiothreitol at 65°C for 1 h, followed by alkylation with 55 mmol/L iodoacetamide at room temperature in the dark for 30 min, after the incubation with 100% acetonitrile. Finally, the gel pieces were washed and dried using a vacuum concentrator. Overnight tryptic digestion was conducted in 50 mmol/L NH_4HCO_3 at 37°C. After in-gel digestion, peptides were extracted with 60% acetonitrile/5% formic acid in an ultrasonic bath. The collected peptide samples were vacuum dried and purified using C18 desalting columns. The eluate was vacuum dried and stored at −20°C for later use. Liquid chromatography-tandem mass spectrometry (MS/MS) data were acquired on a trapped ion mobility spectrometry (tims)TOF Pro mass spectrometer (Bruker). Peptides were loaded and separated successively onto a C18 trap column (75 μm × 2 cm, 3-μm particle size, 100 Å pore size; Thermo Fisher Scientific) and a C18 analytical column (75 μm × 250 mm, 3-μm particle size, 100 Å pore size; Thermo Fisher Scientific). Mobile phase A (H_2O, 0.1% formic acid) and mobile phase B (acetonitrile, 0.1% formic acid) were used to establish the separating gradient. The constant flow rate was set at 300 nL/min. For information-dependent acquisition mode analysis, trapped ion mobility spectrometry function was used, and parallel accumulation–serial fragmentation scan mode was applied: each scan cycle total time was 1.11 s, which consisted of MS1 scan time of 0.1 s and MS2 scan time from precursor of the rest-time MS raw data were analyzed with MaxQuant (V1.6.6) using the Andromeda database search algorithm. Spectra files were searched against the UniProt human proteome database using the following parameters: label-free quantification mode was checked for quantification; variable modifications, methyl (R), dimethyl (R), oxidation (M), and acetyl (protein N-term); fixed modifications, carbamidomethyl (C); digestion, trypsin/P; and matching between runs was used for identification transfer. Search results for both proteins and peptides were filtered with 1% false discovery rate. MS identification of PPARγ methylation sites was performed by SpecAlly Life Technology Co., Ltd., Wuhan, China.

RNA Extraction and Gene Expression Analysis

RNA was isolated from the tissue or cell samples using TRIzol reagent (Invitrogen, 15596018). cDNA was synthesized and quantified by qPCR using commercial kits (Takara, RR036 and RR086) and an ABI 7500 Real-Time PCR system (Thermo Fisher Scientific). Primer pairs are provided in Supplementary Table 1, with 18S as the internal control.

RNA Sequence

RNA sequencing (RNA-seq) was used for total RNA analysis using the MGI platform. Briefly, RNA quality analysis was performed using a NanoPhotometer spectrophotometer, Qubit 3.0 Fluorometer, and Agilent 2100. A complementary cDNA library was then constructed using mRNA enriched with anti-polyA magnetic beads, followed by fragmentation, circularization, and sequencing using DNBSEQ-T7(MGI Tech Co., Ltd.) as 150 base-pair paired-end reads, yielding fastq files filtered for low-quality, N-rich, or adaptor-polluted reads. Reads from the RNA-seq libraries were filtered to remove adapters or low-quality reads. Statistical analysis of data quality and production was performed after filtering to ensure sequencing quality. Gene read counts mapped to the genes or exons were used to determine the reads per kilo base per million mapped reads of each gene. Differential expression analysis, clustering heat map, functional enrichment analysis of general odorant-binding proteins, and Kyoto Encyclopedia of Genes and Genomes (KEGG) pathways were performed using R software.

Luciferase Reporter Assay

Luciferase assays were performed by amplifying the UCP1 promoter from human genomic DNA using PCR and then subcloning it into the pGL3.0-basic vector (Promega, E1751) using an In-Fusion HD cloning kit (Takara, 639648). The

indicated plasmids were cotransfected into HEK293T cells, and the dual-luciferase assay system (Promega) was used to measure cell lysates after 24 h. The following primers were used to amplify the human UCP1 promoter: forward, 5′-GAGCTCTTACGCGTGCTAGCAGCTCTGCAAGCCTGACCTC-3′; reverse, 5′-CAGTACCGGAATGCCAAGCTTGCTCTTCACGCCTGTCCGC-3′.

The Electrophoretic Mobility Shift Assay

The Light Shift Chemiluminescent Electrophoretic Mobility Shift Assay (EMSA) kit (Thermo Fisher Scientific, 20148) was used to detect DNA-protein interactions. The sequences of peroxisome proliferator-activated receptor response element (PPRE) consensus oligonucleotides were as follows: forward, 5′-CAAAACTAGGTCAAAGGTCA-3′; reverse, 5′-GTTTTGATCCAGTTTCCAGT-3′.

Oligonucleotides were labeled with biotin at the 5′-end. The reaction mixture was subjected to PAGE and transferred to nylon membranes after incubation with an oligonucleotide probe for 20 min, which was immediately cross-linked using a ultraviolet transilluminator. Chemiluminescence was then used to detect the bands.

ELISA Analysis

The serum level of insulin was measured with an insulin ELISA kit (Millipore, EZRMI-13K), according to the manufacturer's instructions.

Statistical Analysis

SPSS 23 software (IBM, Armonk, NY) was used for statistical analysis. Densitometry of Western blot bands was quantified with ImageJ software. All data are presented as the mean ± SEM. An unpaired Student two-tailed *t* test was used to compare differences between two groups (normal distribution assumed); otherwise, the Mann-Whitney nonparametric test was used. One-way or two-way ANOVA, followed by the Tukey post hoc test, was performed for multiple group comparisons (equal variance assumed); otherwise, the nonparametric Kruskal-Wallis test was used for further analysis. The energy metabolism data, including VO_2, VCO_2, and heat production, were analyzed by ANCOVA, with body weight as a covariate (22–24). The statistical significance threshold was $P < 0.05$. Three independent replicates were conducted for each cell experiment.

Data Resource and Availability

RNA sequences are available under the BioProject (https://www.ncbi.nlm.nih.gov/bioproject/) ID PRJNA851270. The MS proteomics data have been deposited to the ProteomeXchange Consortium (https://proteomecentral.proteomexchange.org) via the iProX partner repository, with the data set identifier PXD034929. On reasonable request, the corresponding author will provide the information and materials that back up the study's conclusions.

RESULTS

PRMT4 Is Upregulated by Thermogenic Stimuli but Downregulated in Obesity

Our initial studies with Western blot and Real-time qPCR analysis showed that PRMT4 was most abundantly expressed in iWAT compared with other organs and tissues (Fig. 1*A* and *B*). Further analysis of the sequence data from "single-cell atlas of mouse WAT" demonstrated that PRMT4 was ubiquitously expressed among different cell types in adipose tissue (Supplementary Fig. 1*A*) (25). Owing to the essential role of iWAT in adaptive thermogenesis, the expression level of PRMT4 under thermogenic stimulation was explored. A conceivable increase in PRMT4 expression was observed in cold-exposed iWAT (Fig. 1*C*). A similar pattern was noted in the expression profile of UCP1, ADMA, the main form of arginine methylation mediated by PRMT4, and H3R17me2 (a classical methylation substrate of PRMT4) (Fig. 1*E* and *F*). To further confirm the involvement of PRMT4 in thermogenesis, CL316,243 (β3 adrenoceptor agonist) was used. Within expectation, the above-mentioned proteins were also upregulated in CL316,243-treated mature adipocytes differentiated from primary SVF cells of iWAT (Supplementary Fig. 1*B* and *C*). Noteworthily, no change in PRMT1, the predominant member for arginine methylation, was observed in cold-exposed iWAT (Supplementary Fig. 1*D* and *E*), which further confirmed the unique role of PRMT4. The expression of PRMT4 was also explored in the state of obesity, a common metabolic disorder with decreased iWAT browning (2,5). The protein and mRNA levels of PRMT4 were substantially decreased in iWAT of HFD-fed mice, genetically obese (*ob/ob*) mice, and obese patients (Fig. 1*G–N*). In addition, the *PRMT4* mRNA levels in the iWAT of patients were positively correlated with that of *UCP1* and negatively correlated with BMI (Fig. 1*O* and *P*). Collectively, these data indicated that PRMT4 was incorporated in the process of iWAT browning.

It is noteworthy that no changes in *PRMT4* mRNA levels were observed in cold-exposed iWAT (Fig. 1*D*), indicating the involvement of a posttranscriptional mechanism. A previous publication showed that the stability of PRMT4 was disrupted by the E3 ligase S-phase kinase-associated protein 2 (SKP2), whose expression could be inhibited by AMPKα (26). Besides, another study by Peng et al. (27) demonstrated that AMPKα was activated during WAT browning. Consistently, our immunoblotting analysis revealed that cold exposure led to increased PRMT4 and p-AMPKα expression and decreased SKP2 level (Supplementary Fig. 2*A* and *B*). In addition, cold-induced upregulation of PRMT4 was significantly repressed by AAV-mediated SKP2 overexpression in vivo (Supplementary Fig. 2*C* and *D*). Further co-IP assay also revealed that SKP2 overexpression almost abolished cold-stimulated downregulation of the PRMT4 ubiquitination level in iWAT (Supplementary Fig. 2*E*). In addition, overexpression of SKP2 decreased the half-life of PRMT4 protein in cycloheximide-treated HEK293T cells (Supplementary Fig. 2*F* and *G*). Therefore, we speculated that the expression of

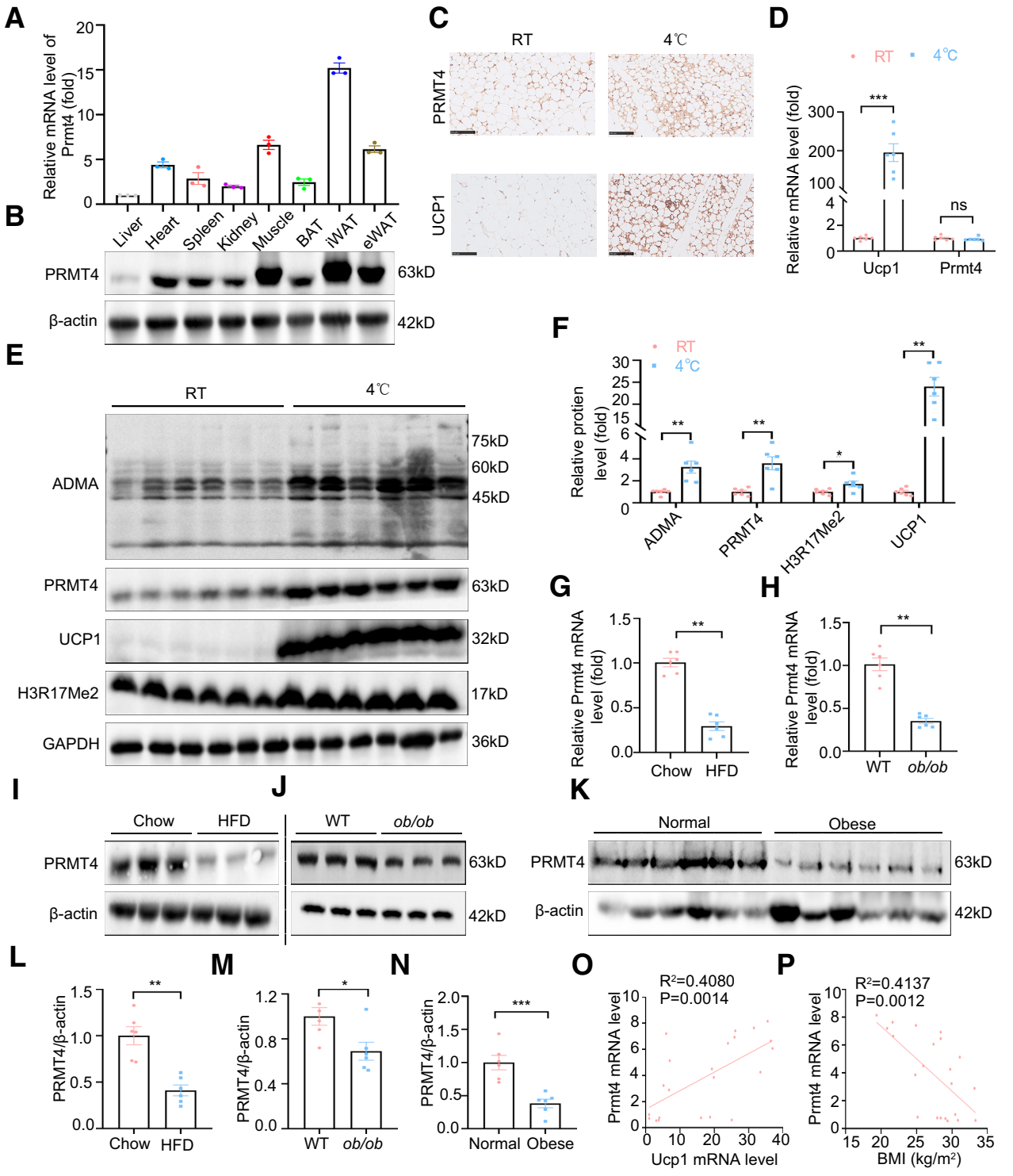

Figure 1—PRMT4 expression is upregulated by thermogenic stimulation and negatively correlates with obesity. Real-time qPCR analysis (*A*) and representative immunoblotting images (*B*) showing the PRMT4 expression profiles in various tissues. *C*–*F*: Mice were maintained at room temperature (RT; 23°C) or in a cold environment (4°C) for 24 h, and iWAT was collected for further analysis. *C*: Immunohistochemical analysis of UCP1 and PRMT4 staining. Scale bar, 100 μm. *D*: Real-time qPCR analysis of the *Ucp1* and *Prmt4* mRNA expression levels. *E*: Representative immunoblotting images of the expression levels of ADMA, PRMT4, UCP1, and H3R17Me2 in iWAT. *F*: Quantitative analysis of the indicated protein expression in panel *E*. *G*: Relative mRNA levels of *Prmt4* in iWAT from HFD-fed mice. *H*: Relative mRNA levels of *Prmt4* in iWAT from *ob/ob* mice. Representative immunoblotting images of the expression levels of PRMT4 in iWAT from HFD-fed mice (*I*) for 12 weeks or *ob/ob* mice (*J*). *K*: Representative immunoblotting images of the expression levels of PRMT4 in WAT from patients. *L*: Quantitative analysis of PRMT4 level in panel *I*. *M*: Quantitative analysis of PRMT4 level in panel *J*. *N*: Quantitative analysis of PRMT4 level in panel *K*. Linear regression analysis of the mRNA level of *Prmt4* with *Ucp1* (*O*) in WAT or with BMI (*P*). Symbols represent individuals. Data are presented as mean ± SEM. $*P < 0.05$, $**P < 0.01$, and $***P < 0.001$; ns, nonsignificant.

PRMT4 was modulated by the AMPKα-SKP2 axis in a cold-exposed scenario.

PRMT4 Overexpression in iWAT Ameliorates HFD-Induced Obesity and Metabolic Dysfunction

Next, the role of PRMT4 in HFD-induced obesity was investigated. Recombinant AAV-NC or AAV-PRMT4 was applied to infect subcutaneous fat pads (Supplementary Fig. 3*A*). Successful transduction of AAV into mature adipocytes of iWAT was verified by immunofluorescence staining and Western blot studies (Fig. 2*A* and Supplementary Fig. 3*B–D*). PRMT4 overexpression attenuated HFD-induced increased body weight when the food intake was comparable (Fig. 2*B* and *C* and Supplementary Fig. 4*A*). Other metabolic disorder-related indexes, including serum levels of triglyceride, free fatty acid, glucose tolerance, insulin sensitivity, and fasting serum insulin, were also disrupted in HFD-fed mice, which were alleviated by PRMT4 overexpression (Fig. 2*D–F* and Supplementary Fig. 4*B–D*). Besides, the weights of iWAT and epididymal WAT (eWAT) were reduced by PRMT4 overexpression in the obese state, while BAT weight was not affected (Fig. 2*G* and *H*). Interestingly, histological analysis demonstrated significantly smaller adipocyte sizes in iWAT, eWAT, and BAT, although PRMT4 overexpression was only observed in iWAT (Fig. 2*I*). The state of liver lipid accumulation, a common obesity-related metabolic disorder, was also investigated. HFD-induced increase in liver weight, lipid content (triglycerides and free fatty acids), and liver lipid deposition was conceivably attenuated by PRMT4 overexpression, whereas no statistical difference in the liver weight-to-body weight ratio was noted (Supplementary Fig. 4*E–I*). Collectively, these results revealed that PRMT4 overexpression in iWAT alleviated HFD-induced obesity and metabolic disorders in vivo.

Owing to the similar amounts of food intake in each group (Supplementary Fig. 4*A*), we hypothesized that PRMT4 might alleviate obesity and metabolic disorders by enhancing energy expenditure. A CLAMS was used to assess energy consumption. The results showed that PRMT4 overexpression resulted in enhanced VO_2, increased VCO_2, and overwhelming heat production compared with HFD-fed control mice (Fig. 2*J–O*). No changes in locomotor activity were observed (Fig. 2*P*). Further analysis revealed that PRMT4 increased the protein level of UCP1 in iWAT (Fig. 2*Q* and *R*). In addition, the mRNA levels of thermogenic genes (*Ucp1*, *Prdm16*, *Cidea*, *Pgc1α*, *Dio2*, and *Elvol3*) were induced by PRMT4 overexpression in HFD-fed mice, whereas the expression of the adipogenic genes (*Pparγ* and *Fabp4*) and lipolytic genes (*Pparα* and *Acox*, but not *Fabp4*) was unchanged (Fig. 2*S*). All in all, these data indicated that PRMT4 overexpression in iWAT ameliorated HFD-induced obesity by promoting energy expenditure.

PRMT4 Promotes Adaptive Thermogenesis

In regard to the fact that PRMT4 accelerated energy expenditure in HFD-fed mice, its role in iWAT browning and adaptive thermogenesis was investigated in a cold-exposure model. The results showed that PRMT4 overexpression resulted in higher rectal temperature, enhanced VO_2, increased VCO_2, and higher heat production compared with cold-primed control mice (Fig. 3*A–H*). Locomotor activity (Fig. 3*I*), body weight, and basal metabolic rate at room temperature when fed a normal chow diet (Supplementary Fig. 5*A–H*) were comparable in each group. H&E staining showed that PRMT4 enhanced brown-like morphology in cold-primed iWAT (Fig. 3*J*). In addition, PRMT4 overexpression attenuated cold-induced disruptions in the mRNA levels of thermogenic genes (*Ucp1*, *Prdm16*, *Cidea*, *Pgc1α*, *Dio2*, and *Elvol3*) in iWAT (Fig. 3*K*). Cold-induced upregulation of UCP1 was also modulated by the expression profile of PRMT4 (Fig. 3*L-N*).

Next, we investigated whether PRMT4 knockdown exhibited the opposite phenotype. AAV-shPRMT4 delivery achieved efficient and specific PRMT4 knockdown in iWAT (Fig. 4*A* and Supplementary Fig. 6*A* and *B*). When subjected to cold exposure, AAV-shPRMT4 mice showed impaired cold tolerance, decreased VO_2, suppressed VCO_2, and lower heat production compared with AAV-shNC mice (Fig. 4*B–I*); however, the locomotor activity (Fig. 4*J*) and body weight, as well as the basal metabolic rate at room temperature when fed a normal chow diet, were not altered (Supplementary Fig. 7*A–H*). Consistent with the CLAMS data, H&E staining showed fewer multilocular fat cells (Fig. 4*K*). Additionally, knockdown of PRMT4 remarkably inhibited the expression of cold-induced thermogenic genes (*Ucp1*, *Prdm16*, *Cidea*, *Pgc1α*, *Dio2*, and *Elvol3*) in iWAT (Fig. 4*L*). Similarly, PRMT4 knockdown in iWAT suppressed cold-induced UCP1 protein expression (Fig. 4*M–O*).

Further, the effect of PRMT4 on BAT and eWAT function was also investigated even when AAV-mediated gene manipulation was conducted only in the iWAT. We found that overexpression of PRMT4 in iWAT exhibited increased UCP1 protein levels in BAT, and the opposite effect was observed when PRMT4 was silenced; however, no significant alteration was observed in eWAT (Supplementary Fig. 8*A–J*). It was reported that metabolic inflammation and angiogenesis also participated in the process of iWAT browning and adaptive thermogenesis (28,29). Therefore, immunofluorescence analysis was performed, and the results showed that macrophage infiltration and capillary density in iWAT were not affected by PRMT4 gain and loss-of-function in vivo (Supplementary Fig. 8*K* and *L*). Whether other relevant thermogenic mechanisms are involved in adaptive thermogenesis needs further in-depth investigation.

In addition, the role of PRMT4 in white-to-beige adipocyte conversion in vitro was also investigated with primary adipocytes that were differentiated from SVF cells isolated from iWAT of WT mice (Supplementary Fig. 9*A*). Our work showed that CL316,243 treatment led to increased expression of Ucp1 and thermogenic markers (*Ucp1*, *Prdm16*, *Cidea*, *Pgc-1α*, *Dio2*, and *Elvol3*) in cells and enhanced nonesterified fatty acid levels in the culture medium, which were promoted by PRMT4 overexpression but attenuated by PRMT4 knockdown (Supplementary Fig. 9*B–I*). Altogether, these data

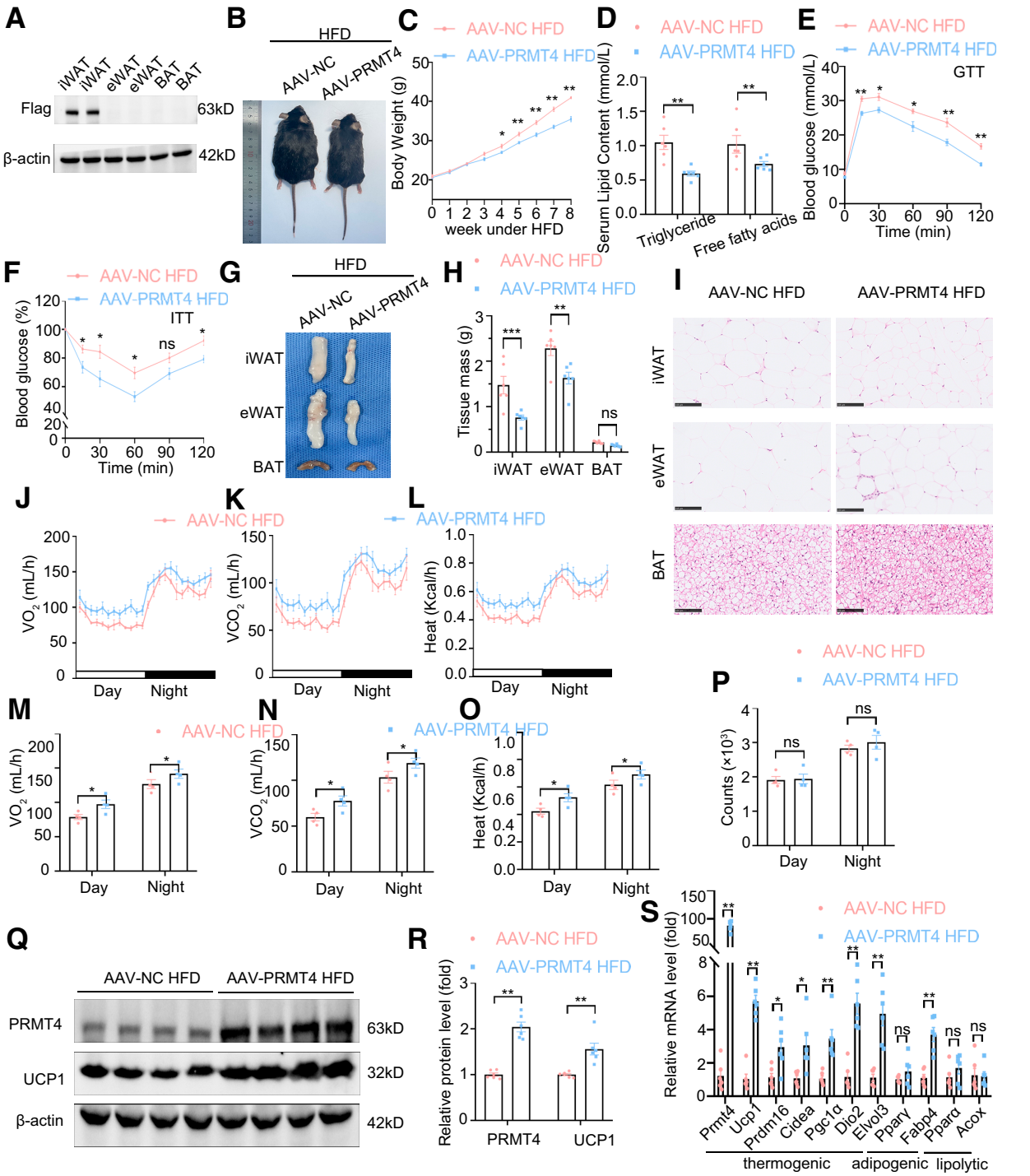

Figure 2—PRMT4 overexpression in iWAT prevents HFD-induced obesity by promoting energy expenditure. AAV-NC or AAV-PRMT4 was subcutaneously injected into the bilateral inguinal areas, and 2 weeks later, the mice received 8 weeks of the HFD. *A*: Representative immunoblotting images show the expression levels of Flag-tagged PRMT4 protein in iWAT, eWAT, and BAT from PRMT4-overexpressed mice. *B*: Gross morphology of mice before sacrifice. *C*: Body weight of the mice. *D*: Serum lipid content (triglycerides and free fatty acids) after 8 weeks of the HFD. *E*: GTT after 6 weeks of the HFD. *F*: ITT after 7 weeks of the HFD. *G*: Gross morphology of the fat pads (iWAT, eWAT, and BAT). *H*: Adipose tissue (iWAT, eWAT, and BAT) weights of mice. *I*: Representative H&E staining of adipose tissues (iWAT, eWAT, and BAT) after 8 weeks of the HFD. Scale bar, 100 μm. The VO_2 (*J*), VCO_2 (*K*), and heat production (*L*) of mice were analyzed after 8 weeks of the HFD. The day/night bar represents a 12-h duration. *M*: Quantitative analysis of VO_2 in panel *J*. *N*: Quantitative analysis of VCO_2 in panel *K*. *O*: Quantitative analysis of heat production in panel *L*. VO_2, VCO_2, and heat production were analyzed by ANCOVA with total body mass as a covariate. *P*: Average values of physical activity. *Q*: Representative immunoblotting images of the expression levels of PRMT4 and UCP1 in iWAT after 8 weeks of the HFD. *R*: Quantitative analysis of the indicated protein expression in panel *Q*. *S*: Relative mRNA levels of thermogenic, adipogenic, and lipolytic genes in iWAT after 8 weeks of the HFD. Data are presented as mean ± SEM. $*P < 0.05$, $**P < 0.01$, and $***P < 0.001$; ns, nonsignificant.

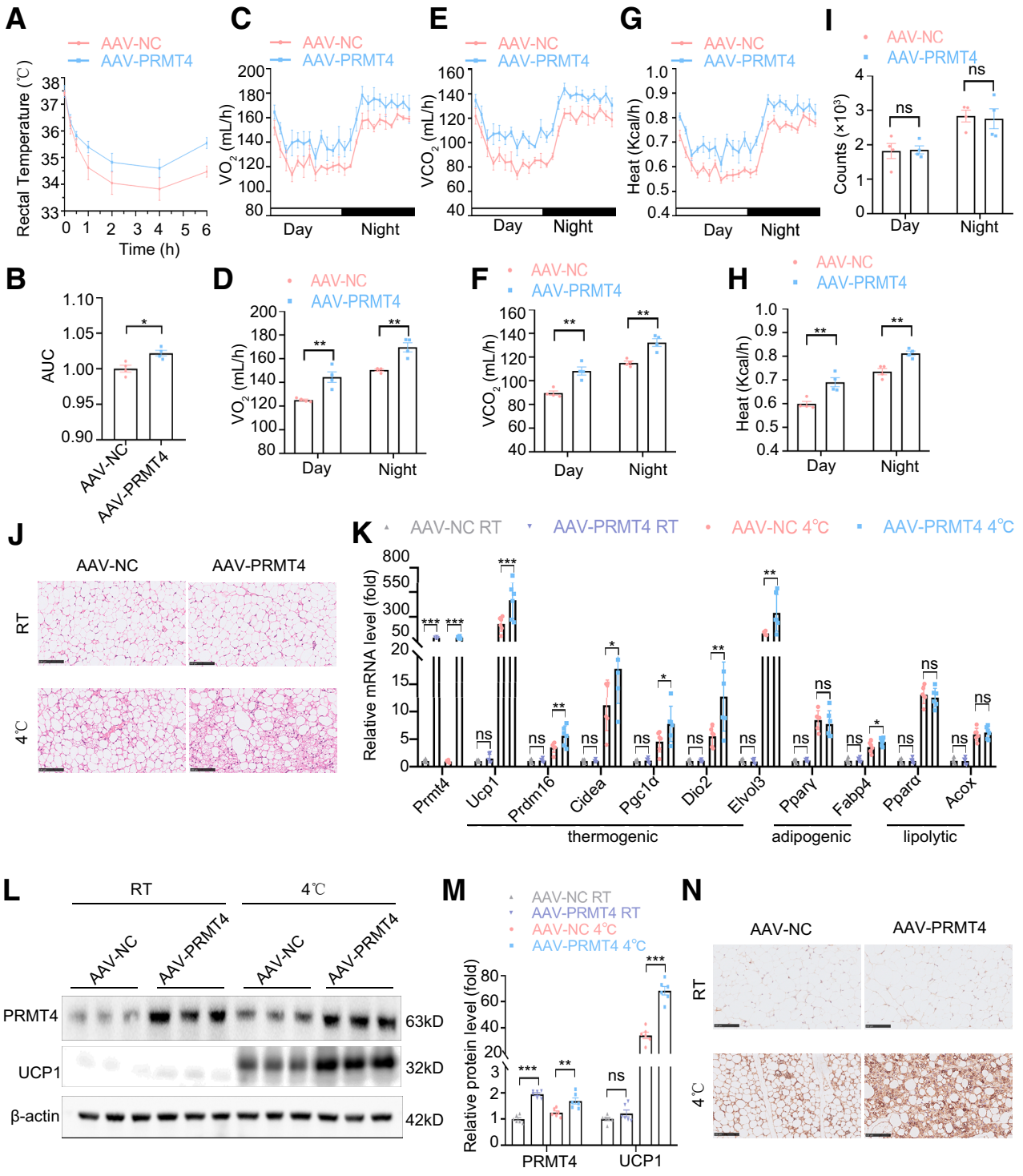

Figure 3—PRMT4 gain-of-function promotes cold-induced browning of iWAT. AAV-NC or AAV-PRMT4 was subcutaneously injected into the bilateral inguinal areas, and 2 weeks later, the mice were subjected to cold exposure (4°C) for 24 h before sacrifice. *A*: The rectal temperature of mice during acute cold exposure (4°C) was monitored in the first 6 h. *B*: Quantitative analysis of relative temperature in panel *A*. AUC, area under the curve. VO_2 (*C*), VCO_2 (*E*), and heat production (*G*) were analyzed. The day/night bar represents a 12-h duration. *D*: Quantitative analysis of VO_2 in panel *C*. *F*: Quantitative analysis of VCO_2 in panel *E*. *H*: Quantitative analysis of heat production in panel *G*. VO_2, VCO_2, and heat production were analyzed by ANCOVA with total body mass as a covariate. *I*: Average values of physical activity. *J*: Representative H&E staining of iWAT sections; scale bar, 100 μm. RT, room temperature. *K*, Relative mRNA levels of thermogenic, adipogenic, and lipolytic genes. *L*: Representative immunoblotting images of the expression levels of PRMT4 and UCP1 in iWAT. *M*: Quantitative analysis of indicated protein expression in panel *L*. *N*: Images show UCP1 immunohistochemistry in iWAT sections; scale bar, 100 μm. Data are presented as mean ± SEM. $^*P < 0.05$, $^{**}P < 0.01$, and $^{***}P < 0.001$; ns, nonsignificant.

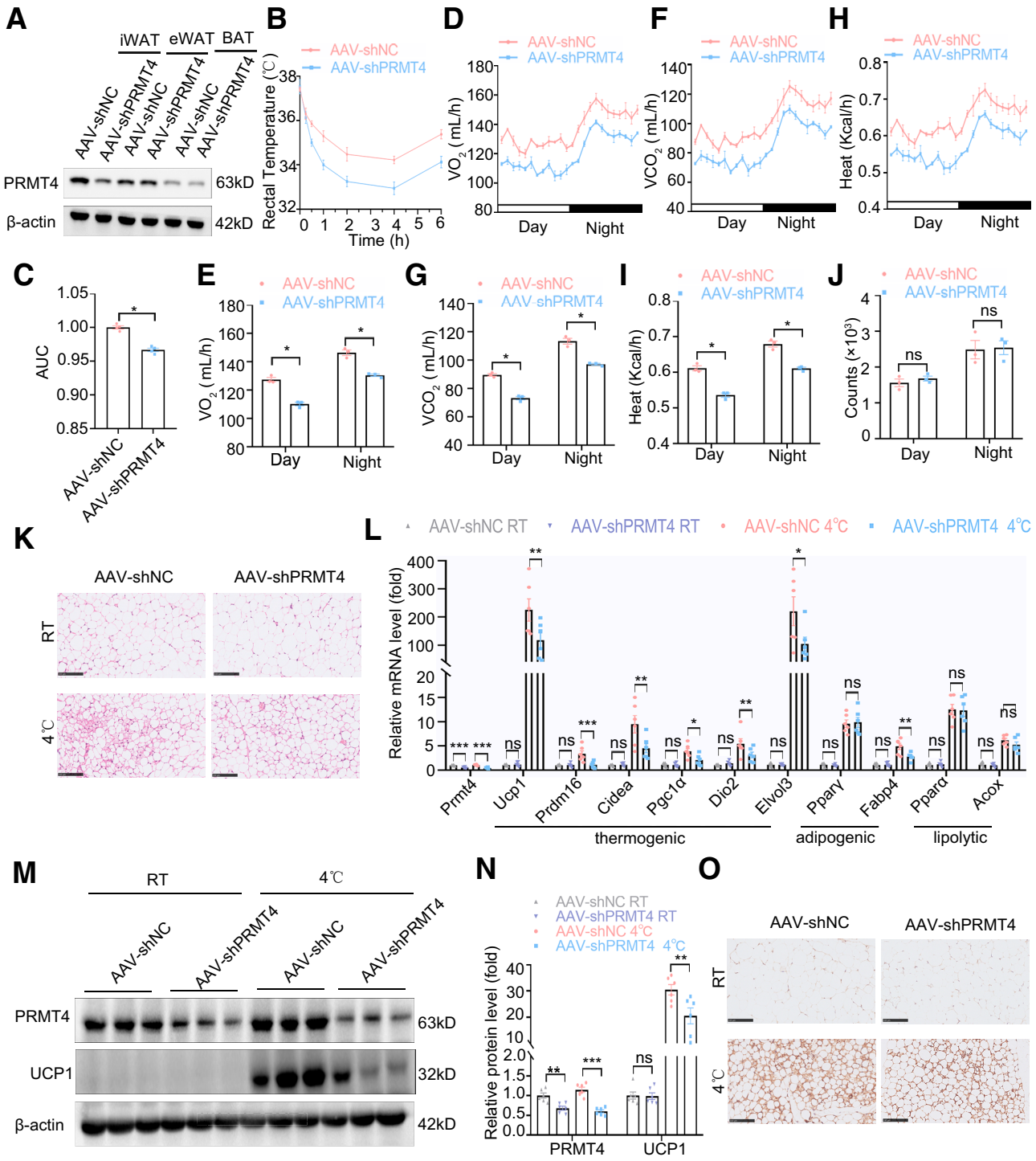

Figure 4—PRMT4 loss-of-function inhibits cold-induced browning of iWAT. AAV-shNC or AAV-shPRMT4 was subcutaneously injected into the bilateral inguinal areas, and 2 weeks later, the mice were subjected to cold exposure (4°C) for 24 h before sacrifice. *A*: Representative immunoblotting images of the expression levels of PRMT4 in iWAT, eWAT, and BAT from mice injected with AAV-shNC or AAV-shPRMT4 subcutaneously into the bilateral inguinal areas. *B*: The rectal temperature of mice during acute cold exposure (4°C) was monitored in the first 6 h. *C*: Quantitative analysis of rectal temperature in panel *B*. AUC, area under the curve. VO_2 (*D*), VCO_2 (*F*), and heat production (*H*) were analyzed. The day/night bar represents a 12-h duration. *E*: Quantitative analysis of VO_2 in panel *D*. *G*: Quantitative analysis of VCO_2 in panel *F*. *I*: Quantitative analysis of heat production in panel *H*. VO_2, VCO_2, and heat production were analyzed by ANCOVA with total body mass as a covariate. *J*: Average values of physical activity. *K*: Representative H&E staining of iWAT sections; scale bar, 100 μm. RT, room temperature. *L*: Relative mRNA levels of thermogenic, adipogenic, and lipolytic genes. *M*: Representative immunoblotting images of the expression levels of PRMT4 and UCP1 in iWAT. *N*: Quantitative analysis of indicated protein expression in panel *M*. *O*: Images showing UCP1 immunohistochemistry in iWAT sections; scale bar, 100 μm. Data are presented as mean ± SEM. *$P < 0.05$, **$P < 0.01$, and ***$P < 0.001$; ns, nonsignificant.

demonstrated that PRMT4 promoted white-to-beige adipocyte conversion to drive adaptive thermogenesis.

PRMT4 Dimethylates PPARγ on Arg240

Previous data revealed that PRMT4 acted as a transcription coactivator to participate in various bioprocesses (13,14); therefore, we hypothesized that PRMT4 might intervene in the transcriptional regulation of thermogenic programs. In this regard, RNA-seq was performed. The overall range and distribution of the fragments per kilo base per million mapped values were comparable among the samples (Supplementary Fig. 10*A*). Principal component analysis study and hierarchical clustering of differentially expressed genes revealed that the global gene expression patterns were conceivably altered upon cold stimulation or PRMT4 overexpression (Supplementary Fig. 10*B* and *C*). Interestingly, KEGG analysis revealed that PPAR signaling occurred among the top 15 significantly affected pathways in the PRMT4-overexpressing state (Fig. 5*A–D*). Therefore, we hypothesized that PRMT4 might interact with PPARγ to modulate iWAT browning, which was subsequently validated by co-IP assay (Fig. 5*E* and Supplementary Fig. 11*A* and *B*). Additionally, co-IP studies with protein truncations revealed that PPARγ bound to the catalytic core domain of PRMT4 (Supplementary Fig. 11*C*). Further studies showed that PPARγ was asymmetrically dimethylated by PRMT4, which was enhanced by cold exposure or PRMT4 overexpression but attenuated by PRMT4 knockdown (Fig. 5*E–G*). In vitro methylation assay with purified PPARγ-Flag and PRMT4-His further demonstrated the direct interaction between PRMT4 and PPARγ (Fig. 5*H*). Moreover, PRMT4-mediated methylation of PPARγ was significantly abolished by TP-064, a selective PRMT4 inhibitor (Fig. 5*H*). The exact methylation site of PPARγ was also investigated. High-performance liquid chromatography-MS/MS analysis indicated that arginine residue 240 of PPARγ was dimethylated (Fig. 5*I*). Notably, a mutation from Arg to Ala on residue 240 almost abrogated the methylation of PPARγ by PRMT4 (Fig. 5*J*). Collectively, these data suggested that PRMT4 directly interacted with PPARγ to catalyze its methylation on arginine residue 240.

PRMT4/PPARγ Axis Recruits PRDM16 to Drive the Thermogenic Transcriptome

Enrichment analysis of Gene Ontology Biological Processes was performed to explore the downstream mechanism of the PRMT4/PPARγ axis in iWAT browning, which showed that the DEGs were significantly enriched in adaptive thermogenesis and fat cell differentiation (Fig. 6*A* and *B* and Supplementary Fig. 12). Previous data showed that PPARγ interacted with PRDM16 and PGC1α to specify the thermogenic gene program (7); therefore, the interaction between PPARγ and PRDM16 or PGC1α was investigated. PRMT4 overexpression enhanced, while PRMT4 knockdown repressed, the interaction between PPARγ and PRDM16 (Fig. 6*C* and *D*). Cold-induced PRDM16 expression was also modulated by the expression profile of PRMT4 (Supplementary Fig. 13*A–D*). In contrast, the interaction between PPARγ and PGC1α was not influenced by PRMT4 overexpression (Fig. 6*F*). PPARγ-recruited PRDM16 was promoted by PRMT4 overexpression, which was considerably attenuated by PPARγ mutation (Arg240, the dimethylation site) (Fig. 6*E*). Importantly, our co-IP experiment showed that PRMT4 did not physically interact with PRDM16 (Supplementary Fig. 14), ruling out the possibility that PRMT4 acted as a linker between PPARγ and PRDM16. Taken together, these results indicated that PRMT4 methylated PPARγ on Arg240 to recruit PRDM16.

EMSA and luciferase reporter assays were conducted to explore the effect of PRMT4 on the transcriptional activity of PPARγ. EMSA analysis showed that methylated PPARγ conceived higher affinity to the PPRE (PPARγ binding sequence) oligonucleotide probe, which was blocked by TP-064 or cold probe administration (Fig. 6*G*). Similarly, luciferase reporter assays also revealed that TP-064 administration or PPRE mutation attenuated PRMT4-mediated PPARγ activation (Fig. 6*H* and *I*). More specifically, PPARγ-mediated UCP1 promoter activation was accelerated by PRMT4 overexpression, which was abolished by PRMT4 inactivation ($PRMT4^{E266Q}$, enzyme-inactive) or PPARγ mutation (Arg240, the dimethylation site) (Fig. 6*J*). Furthermore, the ChIP assay showed that PRMT4 overexpression enhanced the enrichment of PPARγ and PRDM16 on the UCP1 promoter in vivo (Fig. 6*K*). These data showed that PRMT4-catalyzed PPARγ methylation facilitated PRDM16 recruitment, leading to the increased transcriptional activation of UCP1.

PRMT4-Dependent Methylation of PPARγ on Arg240 Is Essential for PRMT4-Mediated iWAT Browning

Our previous results showed that the Arg240 site was important for the PRMT4-induced transactivation of PPARγ. To investigate the role of PRMT4-dependent methylation of PPARγ on Arg240 in iWAT browning, an in vivo experiment was conducted with the application of mutant (AAV-$PPAR\gamma^{R240A}$) and WT AAV-PPARγ. Following 24 h of cold exposure, CLAMS tests and H&E staining suggested that PRMT4 overexpression significantly augments PPARγ-induced energy expenditure and iWAT browning but that these effects were abolished when the PRMT4-mediated methylation site of PPARγ (R240) was mutated from Arg to Ala (Fig. 7*A–H*). Consistently, the AAV-$PPAR\gamma^{R240A}$ mutant reduced the dimethylation level of PPARγ by PRMT4 and exhibited decreased protein level of UCP1 compared with the AAV-PPARγ mice in the scenario of PRMT4 overexpression (Fig. 7*I–L*). Collectively, these results support that PRMT4-dependent methylation of PPARγ on Arg240 is critical for PRMT4-induced iWAT browning.

Pharmaceutical Inhibition of PPARγ Abolished PRMT4-Induced Thermogenic Gene Expression

To further verify that PRMT4-mediated white-to-beige adipocyte reprogramming was PPARγ dependent, T0070907 (a selective inhibitor of PPARγ) was used. CLAMS tests showed that PRMT4-facilitated energy expenditure and cold tolerance

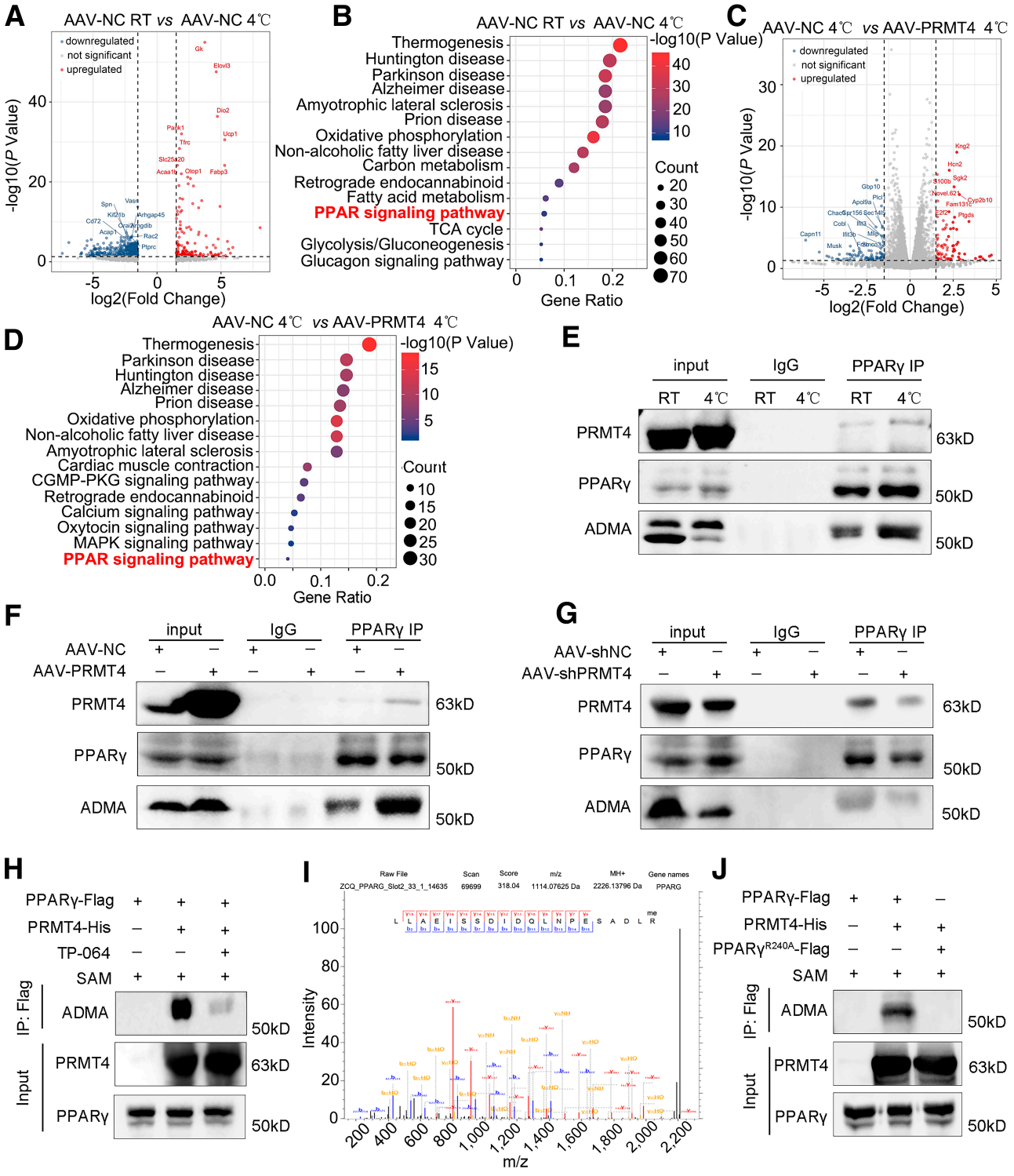

Figure 5—PRMT4 dimethylates PPARγ on Arg240. *A–D*: AAV-NC or AAV-PRMT4 was subcutaneously injected into the bilateral inguinal areas, and 2 weeks later, the mice were subjected to cold exposure (4°C) for 24 h before sacrifice. iWAT from mice at room temperature (RT) or 4°C was collected for RNA-seq analysis. *A* and *C*: Volcano plot shows DGEs (red, upregulated genes; blue, downregulated genes) in iWAT. The vertical dashed black lines in the plot represent log2 normalized fold changes. The horizontal dashed black line represents an adjusted *P* value of 0.05. *B* and *D*: KEGG enrichment analysis of the activated cellular pathways based on the RNA-seq data set using R software. MAPK, mitogen-activated protein kinase; PKG, protein kinase G; TCA, tricarboxylic acid. *E–G*: Mice were hosted at RT or 4°C for 24 h, and iWAT was harvested for co-IP assay. The results showed that PRMT4 interacted with and dimethylated PPARγ. The interaction between PRMT4 and PPARγ was increased under a cold-exposed state or after PRMT4 overexpression (*E* and *F*) but was decreased after PRMT4 knockdown (*G*). *H*: In vitro methylation assay was performed to verify the asymmetrical arginine methylation of PPARγ by PRMT4. *I*: The methylation reaction lysate was subjected to SDS-PAGE gel and Coomassie blue staining. The indicated band (PPARγ) was extracted for high-performance liquid chromatography/MS/MS analysis, and the Arg240 site of PPARγ was identified. *J*: In vitro methylation assay was performed to verify that PRMT4 dimethylates PPARγ on Arg240. A mutation from Arg to Ala at residue 240 almost abrogated the methylation of PPARγ by PRMT4.

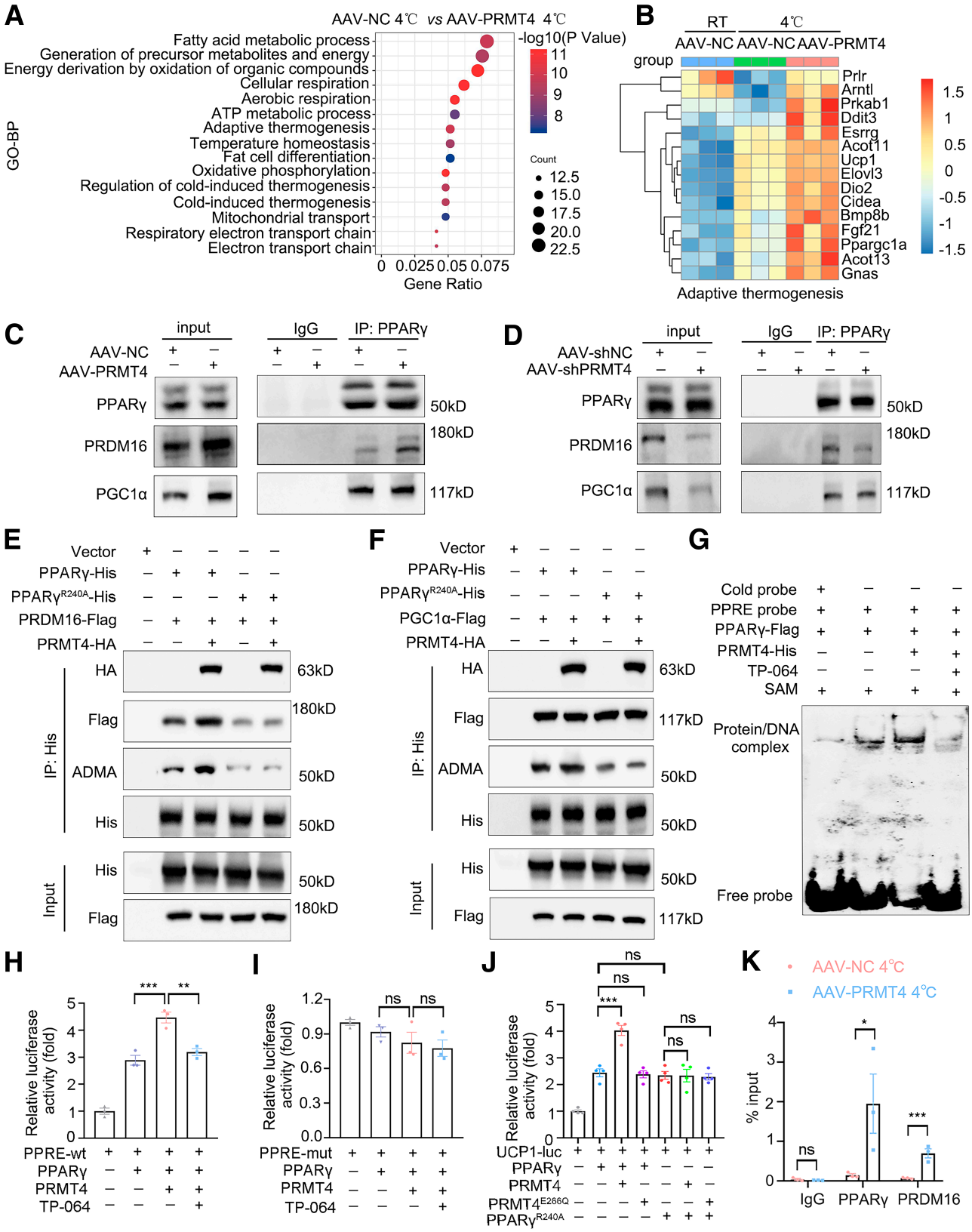

Figure 6—PRMT4-dependent methylation promotes PPARγ-mediated thermogenic gene expression. *A*: Gene Ontology Biological Processes (GO-BP) analysis of DEGs at 4°C in WAT from mice injected with AAV-NC or AAV-PRMT4. RT, room temperature. *B*: Adaptive thermogenesis-related DEGs are shown. *C* and *D*: Co-IP analysis of endogenous interaction between PPARγ and PRDM16 or PGC1α in iWAT from mice after PRMT4 overexpression (*C*) or knockdown (*D*). *E* and *F*: HEK293T cells were transfected with the indicated plasmids, and 48 h later, cell lysates were incubated with anti-IgG or anti-His antibody, followed by immunoblotting with anti-HA, anti-Flag, anti-ADMA, and anti-His antibodies. *G*: Purified PPARγ-Flag protein was incubated with recombinant PRMT4-His protein in the presence or

were significantly repressed by T0070907 (Supplementary Fig. 15*A–I*). Similarly, PPARγ inhibition diminished PRMT4-mediated iWAT browning (Supplementary Fig. 15*J*). In addition, the increased levels of thermogenic genes (*Ucp1*, *Prdm16*, *Cidea*, *Pgc-1α*, *Dio2*, and *Elvol3*) and UCP1 protein expression induced by PRMT4 overexpression were partially reversed by T0070907 administration (Supplementary Fig. 15*K–N*). These findings indicated that the role of PRMT4 on adaptive thermogenesis was mediated by PPARγ.

DISCUSSION

In this study, we uncovered the novel role of PRMT4 in iWAT browning. Initially, our work showed that PRMT4 was abundantly expressed in iWAT, and its expression in iWAT was upregulated upon cold exposure but downregulated in obesity. Further investigation revealed that PRMT4 promoted iWAT browning and facilitated energy expenditure to alleviate HFD-induced obesity and metabolic disorders. Mechanistically, our work presented the initial evidence that PRMT4 interacted with and methylated PPARγ on Arg240 to enhance its transcriptional activity by recruiting the coactivator PRDM16, thus accelerating the thermogenic process.

PRMT4, a type I protein arginine methyltransferase, catalyzes asymmetric dimethylation of its substrates to participate in various pathophysiological processes, including skeletal muscle differentiation (30), cardiomyocyte apoptosis (31), and tumor invasion (32). Interestingly, the role of PRMT4 in metabolic disruptions was recently recognized. For example, it was reported that PRMT4 promoted glycogen metabolism-related gene expression (33) and was involved in insulin secretion by methylating histone H3 (34). Besides, the bioinformatics analysis by Garske et al. (35) identified PRMT4 as a novel variant related to BMI in humans. Furthermore, it was also reported that PRMT4 overexpression was negatively associated with fat pad weight in diabetic mice (18). In line with the previous observations, our work illustrated that the expression of PRMT4 was decreased in the obese state but upregulated upon cold exposure and that PRMT4 overexpression alleviated obesity and its related metabolic disorders. Further investigations showed that the AMPKα-SKP2 axis was involved in the modulation of PRMT4 stability in a cold-exposed scenario, similar to the observation in the state of nutrient starvation (26). Noteworthily, our previous studies demonstrated that the expression of PRMT4 in doxorubicin-induced cardiomyopathy was regulated by Fbxo9 (an E3 ubiquitin ligase) (36), which, however, was not involved in the cold-exposed state. All in all, these data showed that PRMT4 was involved in the alleviation of obesity and its related metabolic disorders.

We next tried to explore the mechanism by which PRMT4 participated in the modulation of obesity and its related metabolic disorders. It has been widely accepted that obesity is a complex disorder resulting from the imbalance of energy homeostasis system, which incorporates genetic, developmental, behavioral, and environmental factors (37). Adipose tissue is an essential organ for energy homeostasis, and its critical role in the pathogenesis of obesity has been intensively investigated (2). Numerous studies reported that WAT browning in response to cold exposure or β3 adrenoceptor stimuli led to mitochondrial biogenesis and the production of UCP1 (38). UCP1 is a unique protein expressed in the inner mitochondrial membrane of brown and beige adipocytes that uncouples oxidative phosphorylation from ATP synthesis to release energy in the form of heat (38). Under normal conditions, catecholamine stimulus is sufficient to induce iWAT browning. However, higher catecholamine concentrations and adipose catecholamine resistance are viewed as the key features of obesity. At the molecular level, catecholamine resistance manifests as a reduction in lipolysis and thermogenesis in response to sympathetic activation in adipose tissue and contributes to the decrease of fuel use in fat cells (39,40). Our results showed that PRMT4 overexpression facilitated UCP1 expression and WAT browning to drive energy consumption in HFD-fed mice or under cold exposure. Noteworthily, 30°C is regarded as thermoneutrality for mice (41), while 22°C (room temperature used in our study) is a mild cold treatment for them. However, no significant difference in energy consumption was observed between PRMT4-overexpressing mice and WT mice at room temperature. One possible explanation was that room temperature-induced cold treatment was quite gentle, which was not sufficient to provoke conceivable phenotype alteration. Similar observation was presented by Chen et al., (42) who reported that Ern1-knockout mice exhibited significantly lower weight gain and energy consumption following 14 weeks of HFD but showed comparable thermogenesis when housed at 22°C (42). Taken together, these results identified that PRMT4 ameliorated HFD-induced obesity by promoting WAT browning.

The next question that needed to be addressed was how PRMT4 modulated the process of iWAT browning. Various aspects of the mechanism have been reported, and recent publications demonstrated the essential role of multiple transcription factors and coactivators (7,11). Our RNA-seq data showed that PPARγ-related signaling was intimately related to PRMT4 overexpression. Similarly, Yadav et al. (20) reported that PRMT4 promoted PPARγ-mediated gene transcription, but that interaction has not been investigated.

absence of TP-064 and then subjected to EMSA. *H* and *I*: PRMT4-mediated PPARγ transactivation was assessed by luciferase assay using the PPRE-wt (*H*) or PPRE-mut (*I*) plasmids, respectively. *J*: Luciferase assay was performed to analyze the effect of PRMT4 on PPARγ-mediated UCP1 promoter activation. *K*: AAV-NC or AAV-PRMT4 was injected into bilateral inguinal areas subcutaneously, and 2 weeks later, after cold exposure (4°C) for 24 h, iWAT was harvested for ChIP assay to analyze the enrichment of PPARγ and PRDM16 on the mouse UCP1 promoter loci. Data are presented as mean ± SEM. $*P < 0.05$, $**P < 0.01$, and $***P < 0.001$; ns, nonsignificant.

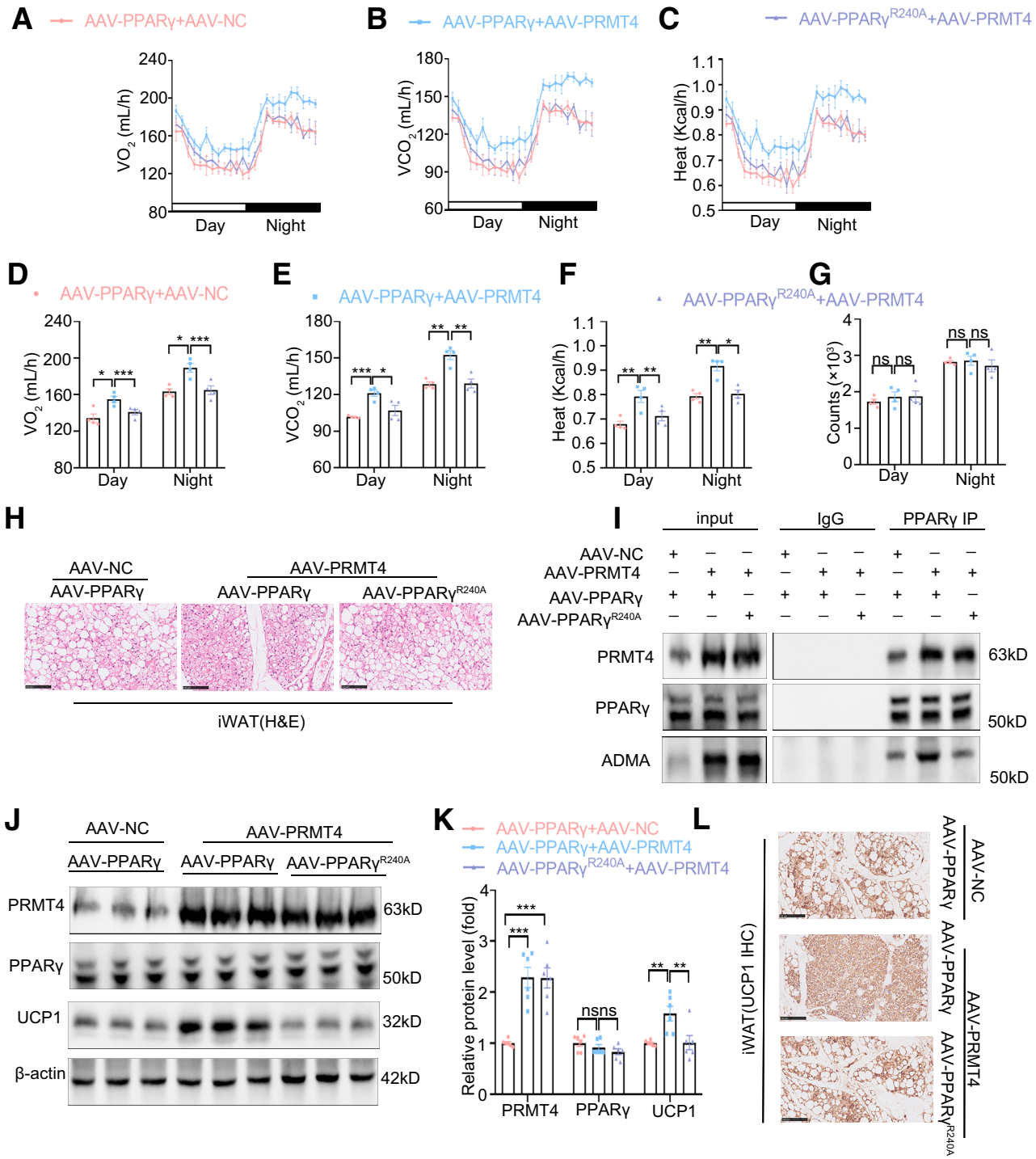

Figure 7—PRMT4-dependent methylation of PPARγ at Arg240 promotes iWAT browning. AAV-PPARγ or mutant AAV-PPARγ^{R240A}, in combination with or without AAV-PRMT4, was subcutaneously injected into the bilateral inguinal areas, and 2 weeks later, mice were subjected to cold exposure (4°C) for 24 h before sacrifice. VO_2 (*A*), VCO_2 (*B*), and heat production (*C*) were analyzed. The day/night bar represents a 12-h duration. *D*: Quantitative analysis of VO_2 in panel *A*. *E*: Quantitative analysis of VCO_2 in panel *B*. *F*: Quantitative analysis of heat production in panel *C*. VO_2, VCO_2, and heat production were analyzed by ANCOVA with total body mass as a covariate. *G*: Average values of physical activity. *H*: Representative H&E staining of iWAT sections; scale bar, 100 μm. *I*: Co-IP assay assessing dimethylation levels of PPARγ in iWAT. *J*: Representative immunoblotting images of the expression levels of PRMT4, PPARγ, and UCP1 in iWAT. *K*: Quantitative analysis of indicated protein expression in panel *J*. *L*: Images showing UCP1 IHC in iWAT sections; Scale bar, 100 μm. Data are presented as mean ± SEM. *$P < 0.05$, **$P < 0.01$ and ***$P < 0.001$; ns, nonsignificant.

Our data revealed that PRMT4 directly interacted with PPARγ via its catalytic core domain to exert its beneficial potency in iWAT browning. PPARγ is a vital therapeutic target for insulin resistance and diabetes, and thiazolidinediones (PPARγ agonists) have been used for the treatment of diabetes in the clinic (43). Recent publications also showed that PPARγ was a master regulator in iWAT browning (6). However, it is noteworthy that the predominant role of PPARγ in adipocytes is context dependent (7). It has been validated that PPARγ interacted with PRDM16 to drive the transcription of thermogenic genes, such as *UCP1*, *Cidea*, *Dio2*, and *Elvol3* (44). However, when TLE3 was recruited to PPARγ, its interaction with PRDM16 was disabled, thus decelerating WAT browning (45). Our present study demonstrated that PRMT4 bound to PPARγ, leading to the enhanced interaction between PPARγ and PRDM16 to facilitate WAT browning. Moreover, our results also showed that PRMT4 promotes adipocyte differentiation in vitro (Supplementary Fig. 16*A* and *B*), which was consistent with a previous study that PRMT4 enhanced adipogenesis (20). It is noteworthy that the expression of PRDM16 was also upregulated by PRMT4 overexpression. A recent study revealed that APPBP2 controlled endogenous PRDM16 protein stability (46); however, our results suggested that PRMT4 had no apparent effect on APPBP2 protein level, indicating that PRMT4 did not regulate PRDM16 expression through APPBP2 (Supplementary Fig. 17*A*–*D*). Previous data showed that PPARγ upregulation or activation promoted the expression of PRDM16 (47), suggesting that PRMT4-induced PRDM16 overexpression might be induced by PPARγ. In this regard, we hypothesized that PRMT4 transactivated PPARγ to promote PRDM16 accumulation, which in turn forms a positive feedback loop to coactivate PPARγ and specifies a thermogenic gene program. However, the mechanism involved needs further investigation. Collectively, these data suggested that PRMT4 interacted with PPARγ to drive iWAT browning.

Finally, the molecular machinery involved in the interaction between PRMT4 and PPARγ was investigated. The transcriptional activity of PPARγ was modulated by various types of posttranslational modifications (12). It was reported that Sirt1 catalyzed the deacetylation of PPARγ on Lys268 and Lys293 to drive PRDM16-mediated BAT gene expression (48) and that sumoylation of PPARγ by PIAS1 enhanced its transcriptional activity in cancer cells (49). Besides, phosphorylation of PPARγ was also reported, which was catalyzed by CDK5 to promote the expression of diabetogenic genes in adipocytes (50). Our present study presented the initial evidence that PPARγ was methylated and that this unique type of posttranscriptional modification was catalyzed by PRMT4. Further in-depth investigations revealed that PRMT4-mediated methylation of PPARγ on Arg240 is essential for PRDM16 recruitment and the thermogenic phenotype. Collectively, these data indicated that PRMT4 methylated PPARγ on Arg240 to participate in the process of iWAT browning.

In conclusion, we uncovered the novel role of PRMT4-mediated PPARγ methylation in iWAT browning, potentially providing a promising target for the treatment of obesity.

Funding. This work was supported by the National Natural Science Foundation of China (grant no. 91949201, 81830014, 81801062, 81974078, 81570530, and 81370550), the Natural Science Foundation of Hubei Province (grant no. 2019ACA133), and Guangzhou Science and Technology Project (grant no. 2023A03J0863, 2023A04J1211).

Duality of Interest. No potential conflicts of interest relevant to this article were reported.

Author Contributions. Y.Z., Y.W., X.L., H.Q., S.Y., C.R., D.F., and D.L. performed the experiments. Y.Z. and X.L. wrote the manuscript. Y. Z. and Y.M. analyzed the data. Y.W., X.L., and L.Y. verified the underlying data. Y.W., F.D., Y.M., and L.Y. revised the manuscript. Y.M., L.Y., and K.H. designed the experiments. K.H. contributed reagents and materials. All authors read and approved the final paper. Y.Z. is the guarantor of this work and, as such, had full access to all the data in the study and takes responsibility for the integrity of the data and the accuracy of the data analysis.

References

1. Blüher M. Obesity: global epidemiology and pathogenesis. Nat Rev Endocrinol 2019;15:288–298
2. Bartelt A, Heeren J. Adipose tissue browning and metabolic health. Nat Rev Endocrinol 2014;10:24–36
3. Cohen P, Kajimura S. The cellular and functional complexity of thermogenic fat. Nat Rev Mol Cell Biol 2021;22:393–409
4. Shao M, Wang QA, Song A, et al. Cellular origins of beige fat cells revisited. Diabetes 2019;68:1874–1885
5. Sakers A, De Siqueira MK, Seale P, Villanueva CJ. Adipose-tissue plasticity in health and disease. Cell 2022;185:419–446
6. Anghel SI, Wahli W. Fat poetry: a kingdom for PPAR gamma. Cell Res 2007;17:486–511
7. Inagaki T, Sakai J, Kajimura S. Transcriptional and epigenetic control of brown and beige adipose cell fate and function. Nat Rev Mol Cell Biol 2016;17:480–495
8. Kawai M, Rosen CJ. PPARγ: a circadian transcription factor in adipogenesis and osteogenesis. Nat Rev Endocrinol 2010;6:629–636
9. Lehrke M, Lazar MA. The many faces of PPARgamma. Cell 2005;123:993–999
10. Tontonoz P, Spiegelman BM. Fat and beyond: the diverse biology of PPARgamma. Annu Rev Biochem 2008;77:289–312
11. Zhang J, Wu H, Ma S, et al. Transcription regulators and hormones involved in the development of brown fat and white fat browning: transcriptional and hormonal control of brown/beige fat development. Physiol Res 2018;67:347–362
12. Brunmeir R, Xu F. Functional regulation of PPARs through post-translational modifications. Int J Mol Sci 2018;19:1738
13. Suresh S, Huard S, Dubois T. CARM1/PRMT4: making its mark beyond its function as a transcriptional coactivator. Trends Cell Biol 2021;31:402–417
14. Yan S, Hu J, Li J, Wang P, Wang Y, Wang Z. PRMT4 drives post-ischemic angiogenesis via YB1/VEGF signaling. J Mol Med (Berl) 2021;99:993–1008
15. Blanc RS, Richard S. Arginine methylation: the coming of age. Mol Cell 2017;65:8–24
16. Wu Q, Schapira M, Arrowsmith CH, Barsyte-Lovejoy D. Protein arginine methylation: from enigmatic functions to therapeutic targeting. Nat Rev Drug Discov 2021;20:509–530
17. Behera AK, Bhattacharya A, Vasudevan M, Kundu TK. p53 mediated regulation of coactivator associated arginine methyltransferase 1 (CARM1) expression is critical for suppression of adipogenesis. FEBS J 2018;285:1730–1744

18. Li Y, Peng M, Zeng T, et al. Protein arginine methyltransferase 4 regulates adipose tissue lipolysis in type 1 diabetic mice. Diabetes Metab Syndr Obes 2020;13:535–544
19. Liu Y, Wang J. C9orf72-dependent lysosomal functions regulate epigenetic control of autophagy and lipid metabolism. Autophagy 2019;15:913–914
20. Yadav N, Cheng D, Richard S, et al. CARM1 promotes adipocyte differentiation by coactivating PPARgamma. EMBO Rep 2008;9:193–198
21. Shu L, Hoo RL, Wu X, et al. A-FABP mediates adaptive thermogenesis by promoting intracellular activation of thyroid hormones in brown adipocytes. Nat Commun 2017;8:14147
22. Mina AI, LeClair RA, LeClair KB, Cohen DE, Lantier L, Banks AS. CalR: a web-based analysis tool for indirect calorimetry experiments. Cell Metab 2018;28:656–666.e1
23. Müller TD, Klingenspor M, Tschöp MH. Revisiting energy expenditure: how to correct mouse metabolic rate for body mass. Nat Metab 2021;3:1134–1136
24. Tschöp MH, Speakman JR, Arch JR, et al. A guide to analysis of mouse energy metabolism. Nat Methods 2011;9:57–63
25. Emont MP, Jacobs C, Essene AL, et al. A single-cell atlas of human and mouse white adipose tissue. Nature 2022;603:926–933
26. Shin HJ, Kim H, Oh S, et al. AMPK-SKP2-CARM1 signalling cascade in transcriptional regulation of autophagy. Nature 2016;534:553–557
27. Peng WQ, Xiao G, Li BY, Guo YY, Guo L, Tang QQ. L-Theanine activates the browning of white adipose tissue through the AMPK/α-ketoglutarate/Prdm16 axis and ameliorates diet-induced obesity in mice. Diabetes 2021;70:1458–1472
28. Villarroya F, Cereijo R, Gavaldà-Navarro A, Villarroya J, Giralt M. Inflammation of brown/beige adipose tissues in obesity and metabolic disease. J Intern Med 2018;284:492–504
29. Xue Y, Petrovic N, Cao R, et al. Hypoxia-independent angiogenesis in adipose tissues during cold acclimation. Cell Metab 2009;9:99–109
30. Chen SL, Loffler KA, Chen D, Stallcup MR, Muscat GE. The coactivator-associated arginine methyltransferase is necessary for muscle differentiation: CARM1 coactivates myocyte enhancer factor-2. J Biol Chem 2002;277:4324–4333
31. Wang Y, Ju C, Hu J, Huang K, Yang L. PRMT4 overexpression aggravates cardiac remodeling following myocardial infarction by promoting cardiomyocyte apoptosis. Biochem Biophys Res Commun 2019;520:645–650
32. Liu J, Feng J, Li L, et al. Arginine methylation-dependent LSD1 stability promotes invasion and metastasis of breast cancer. EMBO Rep 2020;21:e48597
33. Wang SC, Dowhan DH, Eriksson NA, Muscat GE. CARM1/PRMT4 is necessary for the glycogen gene expression programme in skeletal muscle cells. Biochem J 2012;444:323–331
34. Kim JK, Lim Y, Lee JO, et al. PRMT4 is involved in insulin secretion via the methylation of histone H3 in pancreatic β cells. J Mol Endocrinol 2015;54:315–324
35. Garske KM, Pan DZ, Miao Z, et al. Reverse gene-environment interaction approach to identify variants influencing body-mass index in humans. Nat Metab 2019;1:630–642
36. Wang Y, Yan S, Liu X, et al. PRMT4 promotes ferroptosis to aggravate doxorubicin-induced cardiomyopathy via inhibition of the Nrf2/GPX4 pathway. Cell Death Differ 2022;29:1982–1995
37. Schwartz MW, Seeley RJ, Zeltser LM, et al. Obesity pathogenesis: an Endocrine Society Scientific Statement. Endocr Rev 2017;38:267–296
38. Abdullahi A, Jeschke MG. Taming the flames: targeting white adipose tissue browning in hypermetabolic conditions. Endocr Rev 2017;38:538–549
39. Collins S, Daniel KW, Petro AE, Surwit RS. Strain-specific response to beta 3-adrenergic receptor agonist treatment of diet-induced obesity in mice. Endocrinology 1997;138:405–413
40. Reilly SM, Saltiel AR. Adapting to obesity with adipose tissue inflammation. Nat Rev Endocrinol 2017;13:633–643
41. Feldmann HM, Golozoubova V, Cannon B, Nedergaard J. UCP1 ablation induces obesity and abolishes diet-induced thermogenesis in mice exempt from thermal stress by living at thermoneutrality. Cell Metab 2009;9:203–209
42. Chen Y, Wu Z, Huang S, et al. Adipocyte IRE1α promotes PGC1α mRNA decay and restrains adaptive thermogenesis. Nat Metab 2022;4:1166–1184
43. Soccio RE, Chen ER, Lazar MA. Thiazolidinediones and the promise of insulin sensitization in type 2 diabetes. Cell Metab 2014;20:573–591
44. Seale P, Bjork B, Yang W, et al. PRDM16 controls a brown fat/skeletal muscle switch. Nature 2008;454:961–967
45. Villanueva CJ, Vergnes L, Wang J, et al. Adipose subtype-selective recruitment of TLE3 or Prdm16 by PPARγ specifies lipid storage versus thermogenic gene programs. Cell Metab 2013;17:423–435
46. Wang Q, Li H, Tajima K, et al. Post-translational control of beige fat biogenesis by PRDM16 stabilization. Nature 2022;609:151–158
47. Rajakumari S, Wu J, Ishibashi J, et al. EBF2 determines and maintains brown adipocyte identity. Cell Metab 2013;17:562–574
48. Qiang L, Wang L, Kon N, et al. Brown remodeling of white adipose tissue by SirT1-dependent deacetylation of Pparγ. Cell 2012;150:620–632
49. Ohshima T, Koga H, Shimotohno K. Transcriptional activity of peroxisome proliferator-activated receptor gamma is modulated by SUMO-1 modification. J Biol Chem 2004;279:29551–29557
50. Choi JH, Banks AS, Estall JL, et al. Anti-diabetic drugs inhibit obesity-linked phosphorylation of PPARgamma by Cdk5. Nature 2010;466:451–456